Published in final edited form as:
Vet Ophthalmol. 2012 September ; 15(Suppl 2): 13–28. doi:10.1111/j.1463-5224.2012.01045.x.

Optical Coherence Tomography for the Evaluation of Retinal and Optic Nerve Morphology in Animal Subjects: Practical Considerations

Gillian J McLellan[1,2,3,*] and **Carol A Rasmussen**[1]

[1]Department of Ophthalmology & Visual Sciences, School of Medicine and Public Health, University of Wisconsin - Madison, WI 53792, USA

[2]Department of Surgical Sciences, School of Veterinary Medicine, University of Wisconsin - Madison, WI 53792, USA

[3]Eye Research Institute, University of Wisconsin - Madison, WI 53792, USA

Abstract

Optical coherence tomography (OCT) is a non-invasive, non-contact imaging technique capable of producing high-resolution images of the retina and optic nerve. These images provide information that is useful for following the progression and/or resolution of posterior segment disease. Rapid advances in OCT technology allow the acquisition of increasingly detailed images, approaching the original goal of providing *in vivo* histopathology. Increases in scan acquisition speeds and axial resolution enhance the clinical diagnostic value of this modality. Adapting instrumentation designed for use in human patients for use in animals can be challenging. Each species has a unique set of adjustments that need to be made but it is possible to obtain reproducible, high quality OCT images in a variety of animals, including rodents, dogs, cats, pigs and monkeys. Deriving quantitative measurements from OCT instruments is hindered by software algorithm errors in detecting the edges of the distinct retinal layers. These segmentation errors occur in scans of human eyes as well in other species and arise with similar frequency with each of the different OCT instruments. Manual segmentation methods to derive optic nerve head and other structural indices have been developed for several species.

Keywords

Optical coherence tomography; imaging; retina; optic nerve; animal

Introduction

First developed for ocular applications in the 1990s, optical coherence tomography (OCT) is a non-invasive, non-contact, high resolution imaging technique that may be used to study structural changes in the retina and optic nerve head. (1–3) The ability to non-invasively image posterior segment structure allows changes to be monitored longitudinally, thus progression and/or resolution of disease can be documented over time in both clinical and research subjects. In experimental models, OCT imaging offers structural endpoints to test the effects of new treatment strategies, as an important step in the translation of new therapies for blinding diseases from the laboratory to human patients.

[*]Corresponding Author: Dr Gillian J McLellan, Box 3220, F4/3 Clinical Sciences Center, 600 Highland Avenue, Madison, WI 53792, USA, Tel: (+1) 608 263 6649, mclellan@vetmed.wisc.edu.

There are many clinical uses for OCT, and in human ophthalmology this imaging technique has been most widely adopted by vitreo-retinal clinicians for the qualitative assessment of pathologies such as macular edema, epi-retinal membranes (ERM), vitreo-macular traction, macular holes, sub-retinal fluid, photoreceptor layer and/or retinal pigment epithelium (RPE) disruption, and choroidal neovascular membranes (CNV). Macular thickness measurements have also been adopted as a structural endpoint in clinical studies of disorders that affect the macula.(4, 5) Optical coherence tomography also provides quantitative structural measures of inner retina and optic nerve head morphology that are of value in the assessment of patients with glaucoma and other optic neuropathies. However, segmentation issues and other sources of variability in this quantitative data (discussed later in this paper) have thus far limited the widespread adoption of OCT-derived quantitative structural measures as end-points in large-scale glaucoma clinical trials.(6) More recently, modifications in OCT technology have been made that allow high resolution imaging of anterior segment structures including the cornea and anterior chamber angle.(7–10) The focus of this review, however, will be OCT imaging of the posterior segment.

Technology

The principle of operation of OCT, low coherence interferometry, is broadly comparable to ultrasonography, except that it uses light rather than sound. In essence, OCT uses the reflectivity of light waves to produce detailed cross-sectional images of ocular tissues. Unlike ultrasonography, which requires direct contact between probe and tissues or between probe, coupling medium and tissues, OCT does not require any contact with the eye (thus avoiding the potential for tissue compression and/or distortion) and it allows measurement of structures and distances on the sub- 10micron scale, versus the 100micron scale of all but the highest-resolution ultrasonography. OCT systems combine an interferometer with a low coherence light source. The optical beam is split and sent to both the sample (i.e. tissue of interest) and a reference arm (typically a mirror). (Fig. 1) The light reflected by sub-surface features of the tissue is collected by an interferometer. Low coherence optical interferometry involves detection and evaluation of the interference pattern of light reflected from the reference arm interacting with backscattered, reflected light from the tissues of interest. The information obtained about depth and intensity of light reflected from a sub-surface feature is, in turn, utilized to determine spatial dimensions and location of structures within the tissue of interest. These intensity profiles (the axial or A-scans) are then laterally combined to create a transverse, detailed cross-sectional image. (1, 3)

The first widely used commercial OCT system was the Stratus OCT 3 (Carl Zeiss Meditec, Inc.). This system uses time domain (TD-OCT) technology in which the position of the reference mirror is changed and reflected intensity signals are detected from the sample at different depths, sequentially, based on “time of flight”/echo time delay. Since the signals gathered are time-encoded, the system is referred to as a time domain. Newer systems use broadband light sources and gather all backscattered frequencies simultaneously, using a spectrometer, as the reference mirror remains stationary.(11–13). The signal is then analyzed using Fourier analysis, a mathematical transformation in which spatial frequencies are processed to isolate individual components of compound waveforms. This method enables recognition of patterns and mapping of the form of objects, essentially expressing data as a frequency spectrum, with each frequency corresponding to a different tissue depth. These systems are referred to as spectral domain (SD-OCT) or Fourier domain (FD-OCT).

Axial resolution and scan acquisition speed are both dramatically improved with SD-OCT. For example, TD-OCT systems may capture 512 A-scans in 1.28 seconds and provide an axial resolution of 10 microns, whereas SD-OCT systems may capture 1024 A-scans in 0.04 seconds (20,000 to 40,000 per second) with an axial resolution of ~ 5 microns and transverse

resolution of ~ 15um. The higher resolution and denser sampling of SD-OCT increase its diagnostic utility, allowing detection of smaller, more subtle morphologic changes and rapid collection of 3D data sets. The longer scan acquisition time of TD-OCT means that motion artifact can be a problem, even with relatively small ocular movements. Motion artifacts are still possible with SD-OCT but the faster scan time can reduce their frequency. In animal subjects, heavy sedation or general anesthesia are generally required to ensure that the subject is adequately immobilized and limit motion artifacts.

In recent years, a number of different commercially available instruments have entered (and left) the market.(3, 14) Those currently available commercially are listed, and their capabilities summarized, in Table 1. Readers are advised that rapid developments in OCT technology mean that the list of available instruments is likely to change markedly over a span of just a few years. This rapid evolution may work in favor of veterinary clinicians as instruments that quickly become obsolete within the field of human clinical ophthalmology may nevertheless retain their clinical and/or research value for veterinary clinicians at a more affordable price.

Pathology, Longitudinal studies and Structure:Function Relationships

The increased resolution and scan density possible with SD-OCT brings the technology closer to providing non-invasive, *in vivo* histopathology. It has been demonstrated in several species that the distinct layers, visible as alternating bright-dark signals, in highly detailed cross-sectional images of the retina obtained by OCT *in vivo*, can be correlated with retinal layers that are histologically identifiable on light microscopy. (Fig. 2) (15–19) It should be noted that a bright signal previously identified as the inner segment/outer segment junction may actually arise from the ellipsoid region of photoreceptor inner segments.(20)The number of distinct retinal “layers” that are routinely detectable on OCT images varies with species and instrument. An SD-OCT system with resolution capable of imaging the cone mosaic in Zebrafish is now commercially available.(20)

A key benefit of experimental animal models is the ability to correlate *in vivo* OCT scan results with histopathology. These studies have helped to establish the identity of histopathological features corresponding to detectable retinal and optic nerve head sub-surface features on OCT scans. (22) In a cat model of primary congenital glaucoma (PCG) OCT scans were collected at 6-month intervals and compared to age matched controls. Structural differences between normal and PCG cats were pronounced.(Fig. 3) Positive correlations were identified between OCT – derived structural indices such as RNFL thickness and optic nerve axon counts. Similar results were found in an experimental glaucoma model using monkeys.(23) Sub-retinal injection is becoming a more common route for drug delivery to the eye. To document the effects of this dosing method in monkeys, serial OCT, fundus photography and multifocal electroretinography were performed before, and at multiple intervals after, sub-retinal injection of 100 μL of balanced salt solution. (Fig. 4) (24) OCT data were correlated with transient functional losses on multifocal ERG.

Optical coherence tomography can provide valuable information regarding progression or resolution of diseases or injuries. For example, the location, progression and/or resolution of retinal pathology can be followed longitudinally. (Fig. 5). Posterior segment lesions identified on ophthalmoscopy and/or fundus photograph can be better characterized with OCT, which more clearly identifies which retinal layers, if any, are involved. Longitudinal OCT data has also been obtained in several monkey experimental glaucoma model studies, where the damage seen the OCT scans correlated with IOP insult and histopathology (Fig. 6). (15, 23, 25)

Reproducibility and reliability are central to the use of OCT in longitudinal studies. Both have been demonstrated in a variety of macular and optic nerve indications in humans and in animal models (26–30) Reproducibility of results depends on understanding the nature of artifacts that can affect quantitative and qualitative assessment of the OCT data. (31) It is possible to acquire high quality scans in most species but the range of normal variation within differing species has not been well-defined and reproducibility of measurements must be determined for each subject population and instrument. Strategies for quantifying reproducibility (test-retest variability) have been reviewed elsewhere. (32) In longitudinal studies, the effects of age on thickness values must be taken into consideration. In humans, RNFL thickness parameters, especially the inferior and superior quadrants, and macular thickness parameters, except for the central fovea sector, decreased significantly with increasing age.(33) This effect of age may be less of a concern in short-term studies in laboratory animals. Although no significant age-related decline in mean RNFL thickness value was identified within a cohort of 16 normal cats ranging in age from 6 months to 6 years,(34) the potential for an effect of aging should still be considered when conducting long-term longitudinal studies. However, in clinical practice, as many of the animals that present with retinal or optic nerve disease are middle aged or older, age-matched control animals should be evaluated concurrently, if possible.

Practicalities of Image Acquisition

Anesthesia

While newer versions of OCT instruments offer faster scan acquisition speeds, there is still a high probability of movement artifact if animals are not adequately immobilized. Although many of the commonly used anesthesia protocols immobilize the body, few can provide the still eyes needed to acquire high quality scans. Since the animals cannot fixate on a target, as required of human subjects, all alignment needs to be done by the operator, which can substantially lengthen the amount of time required to acquire high quality OCT scans from the area of interest from mere seconds to 10–20 minutes or more. This unpredictability may, in turn, necessitate supplemental doses of sedative, which should also be a consideration in anesthetic choice. In a research setting, subjects are often healthy, young research animals and a single, consistent regimen can generally be adopted quite safely for all subjects. However, in veterinary clinical patients that may be older and may have underlying or concurrent systemic disease, the choice of anesthetic or sedative options may be limited by individual patient safety considerations.

Eye Position & Pupil Dilation

A centrally positioned, immobile eye is a pre-requisite for obtaining quality scans, in addition to limiting movement artifact, the angle of scanning can impact scan quality and quantitative measures (as discussed later in this paper). In cats in a research setting, we typically use intramuscular ketamine (10–20mg/kg) administered in combination with xylazine or a benzodiazipine for heavy sedation, as ketamine results in a centrally positioned eye with a dilated pupil. In young healthy cats these combinations have proven to be safe and effective in our laboratory. However, in a small proportion of subjects, nystagmus persists and can introduce motion artifact. Dogs in particular exhibit downward rotation of their globes in response to anesthesia. Options to help maintain a central, immobile eye for scanning include neuromuscular blockade,(35) retrobulbar saline injections or retrobulbar local anesthetic block. (23) Manual rotation and fixation of the globe to facilitate scanning may be achieved with forceps or atraumatic conjunctival clip electrodes (36). However, manual globe alignment can lead to inadvertent cyclorotation of the globe, resulting in changes in alignment of retinal blood vessels that in turn affect local measures of RNFL and total retinal thickness that need to be taken into consideration in quantitative and

longitudinal studies. Some instruments' software packages offer an "alignment tool" that can compensate for changes in orientation of fundus features. The latter is of great importance during longitudinal studies to detect changes in RNFL thickness values for different quadrants or sectors of the peripapillary region, particularly as retinal blood vessels tend to be co-localized with thicker bundles of ganglion cell axons.(37) Although it may not be necessary for scanning in larger species, e.g. in cats that have received ketamine, application of a mydriatic, such as 0.5–1% tropicamide, is generally recommended.

Corneal Hydration

In contrast to many elderly human patients, most animal subjects will have clear ocular media and as such it is the norm to acquire high quality scans, particularly in research settings. However, even minimal cataract, corneal opacity, inflammatory cells, flare or hemorrhage within aqueous or vitreous can compromise the image quality, resulting in areas of signal dropout, as this is an optical imaging technique, and may even preclude image acquisition. Corneal desiccation should be avoided, as this will negatively impact scan quality.(38) Frequent application of a topical wetting agent (balanced salt solution, or 0.5% carboxymethylcellulose, e.g. Refresh Tears®, Allergan, Irvine, CA) is somewhat effective. However, when imaging multiple subjects of the same species, the best solution is to use plano, rigid gas permeable contact lenses that have been manufactured to conform to the corneal curvature and diameter of the particular species to be imaged. In a comparison of signal strength of OCT images obtained while irrigating the ocular surface with BSS every few seconds, and from the same eyes after application of a rigid, gas permeable contact lens, we found that contact lens application led to a significant increase in mean signal strength, as well as reducing the time taken to acquire high quality scans.

Combination with other Test Procedures

Optical coherence tomography is frequently employed in studies that collect multiple structural and functional measures e.g. ultrasonography, fundus or gonio- photography and electrophysiology. Care should be taken during and between procedures to avoid any corneal drying or epithelial surface damage (see above) and careful consideration given to separating studies into different sessions depending on the compatibility of procedures. For example, as this is an optical imaging technique, any electrophysiological tests should be conducted prior to OCT imaging. Although OCT should be conducted after, rather than preceding electroretinography (ERG), the corneas could potentially be compromised by prior application of ERG contact lens electrodes or drying during the ERG procedure, and image quality can suffer. When evaluating ONH parameters in glaucoma subjects, intraocular pressure (IOP) should be measured prior to and at the conclusion of the scanning session, taking into consideration the potential effects of mydriatics on IOP. (39) If possible, IOP should be within the normal range when scans are acquired as reversible "cupping" due to tissue compliance may confound quantification of ONH morphologic parameters. (40)

Instrument Modifications

The facial features of many domestic species make using built-in chin rests, designed for human patients, problematic. The chin rest structure can interfere with bringing the eyes of an animal subject close enough to the scan head and thus may need to be modified or removed. Fixation targets used in human imaging are often integrated with the chin rest and the electrical connections must be carefully dismantled. For smaller animals, such as rodents, platforms can be manufactured to fit between the bars of the chin rest.

Instruments with moveable scan heads can facilitate image acquisition in animals. The ability to tilt the scan head vertically and swing it horizontally, much as a table-mounted fundus camera, allows the operator to track the eye and gather images in multiple locations

(e.g. macula or *area centralis*, optic nerve head, medullary ray) without repositioning the animal. With anesthetized patients, especially those with an endotracheal tube in place, it is preferable to adjust the instrument to accommodate the patient rather than adjust patient position to accommodate the instrument. However, an advantage to a fixed position scan head is that if the patient is near and perpendicular to the operator, it is relatively easy to make fine adjustments to position. If the patient is directly in front of the operator, it can be difficult to reach around the instrument to reposition the animal and the scanning process may be slowed down unless there is an assistant involved who is dedicated to positioning.

Software can affect the speed of the image acquisition process. With some instruments the OCT image is automatically processed when acquired so even if the operator knows that movement occurred, there is no way to stop the instrument from processing the scan. Some artifacts will not be apparent at time of acquisition. To be sure that high quality scans have been acquired, the operator must leave the scan acquisition mode and go to the analysis mode to verify that the image is artifact free and of sufficient quality.

Species-specific considerations

OCT scanning can be accomplished in a wide variety of animal species. However, each species presents its own challenges:

Rabbits

The unique ocular anatomy of rabbits poses a challenge in positioning, as the optic nerve head and medullary ray are both situated superiorly. Care must be taken to not occlude the airways or put undue strain on the subject's neck. Foam cubes can be manufactured by hand, with cutouts made to support and stabilize the chin. The rabbit optic nerve head is quite wide and has a very deep central cup. Both can be at or near the maximum size capable of fitting in the scan axial and lateral field of view. (Fig. 7) Using software programs designed for human eye structures will likely result in unreliable quantitative values, especially for the RNFL, but most instruments have software features that allow adjustment of segmentation lines and scan circle placement. (41) Custom measurements can be made using caliper features. Fewer retinal structures/layers are demarcated by OCT in rabbits, which may in part relate to optical aberration. The merangiotic vascular pattern of the rabbit fundus limits the number of available landmarks to assist in location of sequential scans in longitudinal studies, (42) due to an absence of retinal blood vessels, except for within the region of the medullary rays. (43)

Mice

The small size of the mouse eye may require use of a corrective lens to compensate for small eye and extremely short focal length required for imaging. Several commercially available instruments have specific rodent attachments for just this purpose. For other instruments, a +2 to +5 Diopter trial lens can be affixed in front of the scan head. Following routine anesthesia and pupil dilation with 1% tropicamide, mice can be placed in cylindrical holders, or conical tubes with the end removed to expose the nose and eyes. Mice can then be positioned by hand or preferably by a modified microscope stage, or similar platform.(Fig. 8) Duration of the scanning procedure should be minimized as safety of anesthesia may be a concern. Reversible cataract formation in anesthetized rodents may impact outcome if the scanning procedure is prolonged and body temperature and corneal hydration are not diligently maintained. (44) (45–47)Very frequent irrigation with balanced salt solution, or application of a methylcellulose ophthalmic demulcent, together with an appropriately sized plano contact lens or coverslip is required. (17, 18, 30) While challenging to scan, the

proliferation of murine models of ocular disease dictates an increasing need for documentation of retinal and optic nerve disease and drug effects in the mouse.

Rats

Good quality scans in rats can be acquired with most commercially available devices without an additional corrective lens. Positioning is similar to that used with mice. A method of stabilizing the head and body, e.g. by means of a customized platform or microscope stage, should be employed, as described for mice. Rats are large enough to place in a small box resting on a stable platform to avoid movement artifacts. Optical coherence tomography has been shown to be a valuable tool to document and validate experimental models of ocular disease in this species. (19, 48–50)

Pigs

Use of OCT has been reported previously in this species. (51) Positioning can be particularly difficult with pigs, including minipigs, given their size, limited neck mobility and ocular conformation, that includes small, deep-set eyes and thick eyelids. However, high quality scans for diagnostic purposes can be acquired. (Fig. 9) As with rabbits, the anatomy of the pig eye is sufficiently different from that of humans that instrument analysis software may not accurately detect retinal layers, in ONH scans in particular. Scans must be carefully examined for errors before tabulating quantitative data.

Dogs and cats

The presence of the reflective *tapetum lucidum* in these species may require adjustment of scan acquisition parameters to achieve even illumination, especially of the fundus reflectance image. If a calm, quiet scanning environment is created, minimal use of sedation may be possible, limiting globe rotation. However, we have found that general anesthesia has been necessary to acquire good quality scans, free from motion artifact. In addition, use of an atraumatic conjunctival clip to stabilize the eye and/or eyelid specula to keep the third eyelid out of the scan path may be used. Previous studies in dogs indicate that whole retinal thickness, RNFL thickness and photoreceptor layer thickness are all greater in the superior (tapetal) than in the inferior (non-tapetal) retina.(35) These authors reported that the thickness measurements on the linear scans were often manually corrected and although the RNFL was correctly delineated in approximately 60% of the peri-papillary scans with the automatic software algorithm, the remaining 40% of these scans had inadequate RNFL delineation. Fortunately, most instruments have software features that allow these manual corrections to be made and several also have 3-D and *en face* visualization features to facilitate qualitative assessments.(Fig. 10) The most common clinical application for posterior segment OCT with companion animal species is to assist in the diagnosis and documentation of treatment efficacy or progression of spontaneous or genetic retinal disease (Fig. 5) as well as glaucoma (Figs. 3and 6). Optical coherence tomography has been used in both dogs and cats in a research setting to visualize sub-retinal implants (52–54); characterize the course of photoreceptor loss and evaluate therapies in retinal degeneration models, (55, 56) (57) and to evaluate the retina and optic nerve head in glaucoma models. (34, 58, 59)

Non-human primates

The retinal structure of the monkey eye is the closest to that of humans, making them very attractive subjects for translational studies. They are commonly used in toxicology and pharmacokinetic drug studies and in experimentally induced models of glaucoma (Figs.5 and 6), CNV and other posterior segment diseases.(22–24) Monkeys are sedated for scanning and a variety of anesthetics can be used, the choice of which depends in part on

what other testing modalities are paired with OCT (e.g. fundus photography, fluorescein angiography or electrodiagnostics). Positioning in an anesthetized non-human primate is best accomplished with a device, e.g. with a bite bar, that holds the head and neck steady, while the animal rests in a prone position in sternal recumbency.

Challenges/limitations

Segmentation

Recognition and segmentation of retinal layers is an ongoing issue in OCT image analysis. Each instrument comes with a proprietary segmentation algorithm that delineates retinal layers in a slightly different way and uses different layers to calculate macular thickness values. Thus, instruments cannot necessarily be used interchangeably and it cannot be assumed that thickness values generated by the software are directly comparable across instruments or even between different iterations of OCT instruments made by the same company.(31, 60–64)(Fig. 11) Different instruments also have different methods of compensating for segmentation errors. While most instruments allow manual segmentation of the line delineating the RPE and RNFL, whether or not this is feasible depends on how many individual lines need to be adjusted. For example, if 128 lines in a macular cube scan need to be manually adjusted the personnel time required might be prohibitive.

Segmentation errors and other errors impacting thickness calculations

The most common segmentation error in animal models is misidentification of the outer retinal layers,(Fig. 14) whereby the software-generated segmentation line does not follow the contour of the RPE. Inner retina misidentification is much less common but can occur when debris in the vitreous is reflective enough to be identified as the inner limiting membrane (ILM). The percentage of scans with segmentation errors is likely to be greater in subjects with a relative lack of pigment in their RPE and choroid. These errors seem to occur with greater frequency in macular cube scans and are an important consideration as sub-albinotic and albino animals are commonly utilized in laboratory studies. These errors may in part be due to enhanced visualization of additional sub-surface, choroidal structures (as seen in the Siamese cats depicted in Figs. 3 and 5A, in contrast to normally pigmented cats, as in Fig 5B)s). or to increased back-scatter of light, and can also be problematic in humans with albinisim. (65) Off -center fixation, a source of segmentation artifact in humans (31), can occur in animal imaging as a byproduct of eye movement and often results in inaccurate thickness measurements of the area *centralis* or fovea. In animal subjects operator skill is required to compensate for lack of fixation. In addition, the circle defining the optic nerve head may not be centered (Fig. 12D) and the line signifying the RNFL layer may be inaccurately drawn. The scan angle should also be evaluated, as tilted rather than “flat” scans indicate that the retinal or ONH surface was not perpendicular to the scanning beam, as is assumed in thickness calculations. (66) All of these image problems affect the numeric thickness values, so if quantitative data is important, inclusion/exclusion criteria need to be defined and each scan carefully evaluated. While artifacts such as RPE and ILM layer segmentation errors and decentration can often be overcome using the manual adjustment features present in most SD-OCT software, artifacts such as scan registration errors still demand operator skill to identify so that scans can be re-acquired.(67)

Most OCT instruments have a circular scan designed to measure RNFL thickness around the optic nerve head. The fixed size (3.4–3.5mm diameter) and round shape of the circle scan is designed for humans and it may not accurately reflect the RNFL anatomy of other species. (Figs. 8 and 11) Even if the circle is not sized appropriately for the subject species, the images may still allow qualitative assessment and may still be useful for assessing longitudinal change. Thickness values for the RNFL are dependent on the location of the

OCT scan circle so registration of scans is essential for thickness measurement reproducibility and longitudinal examination.(68, 69) Opacities in the ocular media, including cataract and corneal lesions can have a profound effect on signal strength and contribute to areas of signal dropout that are often associated with errors in segmentation. Myopia and globe axial length can also affect the incidence of scan artifacts as well as reducing RNFL thickness values and altering thickness sectoral distribution in humans. (70–72) General scan quality, reproducibility and segmentation accuracy may be negatively impacted by ocular diseases such as glaucoma or uveitis. (73) Although in many cases this impact is minor and can be overcome by operator skill so that OCT images of diagnostic quality may still be obtainable, the resulting images should be evaluated carefully for the presence of artifacts and segmentation errors before accepting quantitative data derived from them.

Refinements to the proprietary segmentation algorithms are ongoing for all of the OCT instruments and a number of research groups are also working on enhancing segmentation algorithm accuracy and thus quantitative analysis via computer-aided grading/retinal boundary detection methodologies. (74–76) In some situations, the implications/nuances of the data are better captured by creation of a unique, custom algorithm or manual system of measurement. (25, 77–79)

Scan quality

Each OCT instrument has a unique method of assessing scan quality. Most use a combination of intensity level of the signal along with the uniformity of the signal within a scan. Scans should be evaluated by the operator *during* the scanning session, to ensure that scans at least meet pre-determined requirements for signal strength and absence of areas of signal drop out. Similar to the situation in human glaucoma patients, we have found that mean RNFL thickness in cats is significantly affected by scan signal strength, and this effect should be taken into account when comparing numeric values between scans of different quality.(80, 81)

Future Directions in OCT imaging

Ongoing improvements in OCT imaging include increased use of image registration techniques to better enable comparisons between visits; eye tracking to remove motion error, and frame averaging to enhance contrast and remove image speckle.(27) Disease-specific software is in development for human subjects, including glaucoma progression algorithms centered on macular ganglion cell-inner plexiform layer (GCIPL) thickness (82) and automated algorithms for drusen assessment in age related macular degeneration.(29, 83) Use of OCT is also moving into the surgical realm, with microscope mounted OCT systems for intraoperative imaging.(84) Investigators have combined an operating microscope with an SD-OCT unit to enable wide-field, non-contact, real-time, cross-sectional visualization of retinal structures to facilitate vitreo-retinal surgery. (85, 86)

OCT is also being combined with adaptive optics (AO). These experimental systems may offer reproducible cross-sectional views of RNFL axonal bundles in glaucoma subjects,(87) and may allow quantification of integrity of the photoreceptor mosaic overlying drusen in patients with age-related macular degeneration.(88) Another combination system could allow correlation of AO-SLO images of the photoreceptor mosaic with retinal layers from an AO-OCT B-scan image so that quantitative evaluation of photoreceptor densities, as determined by AO, could be combined with OCT retinal layer thickness or intensity profiles, with the maps for each co-registered. This combination of quantitative data and visualization for qualitative assessment has the potential to greatly enhance clinical diagnosis and monitoring of retinal diseases.(89)

Enhancing Depth of Visualization

Swept source OCT (SS-OCT) systems mostly work at the 1050–1060 nm range, in contrast to SD-OCT technologies that operate at a broader bandwidth with a wavelength of ~850 nm. Using a photodetector to sweep a narrow-bandwidth source through a broad range of frequencies, SS-OCT offers greater scanning speed and less signal drop out with depth. This, enhanced depth penetration allows better visualization of the choroid, sclera, and lamina cribrosa but with lower axial resolution than provided by SD-OCT. (90) A similar improvement in the detection of deeper structures, such as the lamina cribrosa, can also be achieved with modifications to conventional SD-OCT software by changing the position of the reference arm. A number of commercially available SD-OCT instruments now offer an "Enhanced Depth Imaging" mode. (91)

Blood flow studies

Elucidating the role of blood flow in ocular disease is another area where strides are being made using OCT instruments. Altered retinal and/or choroidal blood flow has been implicated in a variety of different ocular diseases including glaucoma, diabetic retinopathy and age-related macular degeneration. Doppler OCT instruments are in development that could enable *in vivo* volumetric imaging of retinal vasculature and quantitation of retinal blood flow. Researchers using a swept source/Fourier domain OCT, operating in the 1050-nm wavelength range with an axial scan rate of 200 kHz, were able to visualize retinal and choroidal vasculature in 3D, calculate vessel area and measure absolute flow in single vessels as well as total retinal blood flow.(92) In another pilot study, normal subjects and glaucomatous patients and patients with diseases of the optic nerve or retinal vasculature were scanned with one of two different 840nm wavelength, spectrometer based Doppler OCT systems. Eyes with glaucoma and vascular disease showed significantly decreased retinal blood flow compared with normal eyes. (93)

In summary, reproducible, high quality scans can be obtained across a wide range of animal species for clinical or research applications, using commercially available, human clinical instrumentation. Clear ocular media and young age facilitate scan acquisition in most animal models. Several instruments also offer rodent specific attachments to facilitate scan acquisition and provide more accurate quantitative retinal thickness values in those species. Software designed for human ocular structures does not always provide accurate quantitative values in animal subjects but a variety of software tools are included with most systems that allow manual compensation for human software algorithm errors. A key advantage offered by OCT in the veterinary ophthalmology clinic is the ability to obtain a non-invasive "biopsy" of posterior segment lesions. These lesions can be visualized and qualitatively assessed with OCT technology and followed over time. Provided that instrument and software limitations are taken into consideration, OCT offers the potential to improve diagnostic accuracy. Assuming reproducibility of measurements has been defined, this imaging modality can provide valuable longitudinal quantitative information about treatment efficacy and/or progression of optic nerve or retinal disease in animal subjects.

Acknowledgments

Support/Acknowledgements:

Supported by NIH grant numbers K08EY018609 and NEI core grant P30EY0016665; a Rapid Response Initiative Grant from the University of Wisconsin Eye Research Institute, and by an unrestricted award from Research to Prevent Blindness to the Department of Ophthalmology and Visual Sciences, University of Wisconsin-Madison. The authors are grateful to Professor I. D. Duncan; Comparative Ophthalmic Research Laboratories (CORL) and Ocular Services On Demand (OSOD, LLC) for allowing access to equipment used in acquiring a number of images presented in this review.

References

1. Huang D, Swanson EA, Lin CP, Schuman JS, Stinson WG, Chang W, et al. Optical coherence tomography. Science. 1991; 254(5035):1178–81. Epub 1991/11/22. [PubMed: 1957169]
2. Hee MR, Izatt JA, Swanson EA, Huang D, Schuman JS, Lin CP, et al. Optical coherence tomography of the human retina. Archives of ophthalmology. 1995; 113(3):325–32. Epub 1995/03/01. [PubMed: 7887846]
3. Gabriele ML, Wollstein G, Ishikawa H, Kagemann L, Xu J, Folio LS, et al. Optical coherence tomography: history, current status, and laboratory work. Investigative ophthalmology & visual science. 2011; 52(5):2425–36. Epub 2011/04/16. [PubMed: 21493951]
4. Csaky KG, Richman EA, Ferris FL 3rd . Report from the NEI/FDA Ophthalmic Clinical Trial Design and Endpoints Symposium. Investigative ophthalmology & visual science. 2008; 49(2):479–89. Epub 2008/02/01. [PubMed: 18234989]
5. Fung AE, Lalwani GA, Rosenfeld PJ, Dubovy SR, Michels S, Feuer WJ, et al. An optical coherence tomography-guided, variable dosing regimen with intravitreal ranibizumab (Lucentis) for neovascular age-related macular degeneration. American journal of ophthalmology. 2007; 143(4): 566–83. Epub 2007/03/28. [PubMed: 17386270]
6. Weinreb RN, Kaufman PL. Glaucoma research community and FDA look to the future, II: NEI/FDA Glaucoma Clinical Trial Design and Endpoints Symposium: measures of structural change and visual function. Investigative ophthalmology & visual science. 2011; 52(11):7842–51. Epub 2011/10/06. [PubMed: 21972262]
7. Izatt JA, Hee MR, Swanson EA, Lin CP, Huang D, Schuman JS, et al. Micrometer-scale resolution imaging of the anterior eye in vivo with optical coherence tomography. Archives of ophthalmology. 1994; 112(12):1584–9. Epub 1994/12/01. [PubMed: 7993214]
8. Doors M, Berendschot TT, de Brabander J, Webers CA, Nuijts RM. Value of optical coherence tomography for anterior segment surgery. Journal of cataract and refractive surgery. 2010; 36(7): 1213–29. Epub 2010/07/09. [PubMed: 20610103]
9. Konstantopoulos A, Hossain P, Anderson DF. Recent advances in ophthalmic anterior segment imaging: a new era for ophthalmic diagnosis? The British journal of ophthalmology. 2007; 91(4): 551–7. Epub 2007/03/21. [PubMed: 17372341]
10. Mireskandari K, Tehrani NN, Vandenhoven C, Ali A. Anterior segment imaging in pediatric ophthalmology. Journal of cataract and refractive surgery. 2011; 37(12):2201–10. Epub 2011/11/24. [PubMed: 22108115]
11. Wojtkowski M, Leitgeb R, Kowalczyk A, Bajraszewski T, Fercher AF. In vivo human retinal imaging by Fourier domain optical coherence tomography. Journal of biomedical optics. 2002; 7(3):457–63. Epub 2002/08/15. [PubMed: 12175297]
12. Wojtkowski M, Bajraszewski T, Targowski P, Kowalczyk A. Real-time in vivo imaging by high-speed spectral optical coherence tomography. Optics letters. 2003; 28(19):1745–7. Epub 2003/09/30. [PubMed: 14514087]
13. Townsend KA, Wollstein G, Schuman JS. Imaging of the retinal nerve fibre layer for glaucoma. The British journal of ophthalmology. 2009; 93(2):139–43. Epub 2008/11/26. [PubMed: 19028735]
14. Kiernan DF, Mieler WF, Hariprasad SM. Spectral-domain optical coherence tomography: a comparison of modern high-resolution retinal imaging systems. American journal of ophthalmology. 2010; 149(1):18–31. Epub 2010/01/28. [PubMed: 20103039]
15. Drexler W, Fujimoto JG. State-of-the-art retinal optical coherence tomography. Progress in retinal and eye research. 2008; 27(1):45–88. Epub 2007/11/27. [PubMed: 18036865]
16. Ruggeri M, Wehbe H, Jiao S, Gregori G, Jockovich ME, Hackam A, et al. In vivo three-dimensional high-resolution imaging of rodent retina with spectral-domain optical coherence tomography. Investigative ophthalmology & visual science. 2007; 48(4):1808–14. Epub 2007/03/29. [PubMed: 17389515]
17. Huber G, Beck SC, Grimm C, Sahaboglu-Tekgoz A, Paquet-Durand F, Wenzel A, et al. Spectral domain optical coherence tomography in mouse models of retinal degeneration. Investigative ophthalmology & visual science. 2009; 50(12):5888–95. Epub 2009/08/08. [PubMed: 19661229]

18. Knott EJ, Sheets KG, Zhou Y, Gordon WC, Bazan NG. Spatial correlation of mouse photoreceptor-RPE thickness between SD-OCT and histology. Experimental eye research. 2011; 92(2):155–60. Epub 2010/11/03. [PubMed: 21035444]
19. Yamauchi Y, Yagi H, Usui Y, Kimura K, Agawa T, Tsukahara R, et al. Biological activity is the likely origin of the intersection between the photoreceptor inner and outer segments of the rat retina as determined by optical coherence tomography. Clin Ophthalmol. 2011; 5:1649–53. Epub 2011/12/17. [PubMed: 22174571]
20. Spaide RF, Curcio CA. Anatomical correlates to the bands seen in the outer retina by optical coherence tomography: literature review and model. Retina. 2011; 31(8):1609–19. Epub 2011/08/17. [PubMed: 21844839]
21. http://www.bioptigen.com/. [cited 2012 March 9].
22. Strouthidis NG, Grimm J, Williams GA, Cull GA, Wilson DJ, Burgoyne CF. A comparison of optic nerve head morphology viewed by spectral domain optical coherence tomography and by serial histology. Investigative ophthalmology & visual science. 2010; 51(3):1464–74. Epub 2009/10/31. [PubMed: 19875649]
23. Schuman JS, Pedut-Kloizman T, Pakter H, Wang N, Guedes V, Huang L, et al. Optical coherence tomography and histologic measurements of nerve fiber layer thickness in normal and glaucomatous monkey eyes. Investigative ophthalmology & visual science. 2007; 48(8):3645–54. Epub 2007/07/27. [PubMed: 17652734]
24. Nork TM, Murphy CJ, Kim CB, Ver Hoeve JN, Rasmussen CA, Miller PE, et al. Functional and anatomic consequences of subretinal dosing in the cynomolgus macaque. Archives of ophthalmology. 2012; 130(1):65–75. Epub 2011/09/14. [PubMed: 21911651]
25. Strouthidis NG, Fortune B, Yang H, Sigal IA, Burgoyne CF. Longitudinal change detected by spectral domain optical coherence tomography in the optic nerve head and peripapillary retina in experimental glaucoma. Investigative ophthalmology & visual science. 2011; 52(3):1206–19. Epub 2011/01/11. [PubMed: 21217108]
26. Mwanza JC, Chang RT, Budenz DL, Durbin MK, Gendy MG, Shi W, et al. Reproducibility of peripapillary retinal nerve fiber layer thickness and optic nerve head parameters measured with cirrus HD-OCT in glaucomatous eyes. Investigative ophthalmology & visual science. 2010; 51(11):5724–30. Epub 2010/06/25. [PubMed: 20574014]
27. Chin EK, Sedeek RW, Li Y, Beckett L, Redenbo E, Chandra K, et al. Reproducibility of Macular Thickness Measurement Among Five OCT Instruments: Effects of Image Resolution, Image Registration, and Eye Tracking. Ophthalmic surgery, lasers & imaging: the official journal of the International Society for Imaging in the Eye. 2012; 43(2):97–108. Epub 2011/12/29.
28. Leung CK, Yu M, Weinreb RN, Ye C, Liu S, Lai G, et al. Retinal Nerve Fiber Layer Imaging with Spectral-Domain Optical Coherence Tomography A Prospective Analysis of Age-Related Loss. Ophthalmology. 2012 Epub 2012/01/24.
29. Chiu SJ, Izatt JA, O'Connell RV, Winter KP, Toth CA, Farsiu S. Validated automatic segmentation of AMD pathology including drusen and geographic atrophy in SD-OCT images. Investigative ophthalmology & visual science. 2012; 53(1):53–61. Epub 2011/11/01. [PubMed: 22039246]
30. Gabriele ML, Ishikawa H, Schuman JS, Bilonick RA, Kim J, Kagemann L, et al. Reproducibility of spectral-domain optical coherence tomography total retinal thickness measurements in mice. Investigative ophthalmology & visual science. 2010; 51(12):6519–23. Epub 2010/06/25. [PubMed: 20574022]
31. Ho J, Sull AC, Vuong LN, Chen Y, Liu J, Fujimoto JG, et al. Assessment of artifacts and reproducibility across spectral- and time-domain optical coherence tomography devices. Ophthalmology. 2009; 116(10):1960–70. Epub 2009/07/14. [PubMed: 19592109]
32. Feuer W. Quantifying the reproducibility of instruments in glaucoma imaging. Journal of Current Glaucoma Practice. 2008; 2(2):1–5.
33. Sung KR, Wollstein G, Bilonick RA, Townsend KA, Ishikawa H, Kagemann L, et al. Effects of age on optical coherence tomography measurements of healthy retinal nerve fiber layer, macula, and optic nerve head. Ophthalmology. 2009; 116(6):1119–24. Epub 2009/04/21. [PubMed: 19376593]

34. Seo, K.; CAR; Finch, AK.; Xiong, K.; Kaufman, PL.; McLellan, GJ., editors. SD-OCT Imaging of the Retina and Optic Nerve in Normal and Glaucomatous Cats 2010 Annual Meeting Assoc Res Vis Ophthalmol. Fort Lauderdale, FL: 2010.
35. Hernandez-Merino E, Kecova H, Jacobson SJ, Hamouche KN, Nzokwe RN, Grozdanic SD. Spectral domain optical coherence tomography (SD-OCT) assessment of the healthy female canine retina and optic nerve. Veterinary ophthalmology. 2011; 14(6):400–5. Epub 2011/11/05. [PubMed: 22050777]
36. Rosolen SG, Lamory B, Harms F, Sahel JA, Picaud S, LeGargasson JF. Cellular-resolution in vivo imaging of the feline retina using adaptive optics: preliminary results. Veterinary ophthalmology. 2010; 13(6):369–76. Epub 2010/12/25. [PubMed: 21182721]
37. Hood DC, Fortune B, Arthur SN, Xing D, Salant JA, Ritch R, et al. Blood vessel contributions to retinal nerve fiber layer thickness profiles measured with optical coherence tomography. Journal of glaucoma. 2008; 17(7):519–28. Epub 2008/10/16. [PubMed: 18854727]
38. Stein DM, Wollstein G, Ishikawa H, Hertzmark E, Noecker RJ, Schuman JS. Effect of corneal drying on optical coherence tomography. Ophthalmology. 2006; 113(6):985–91. Epub 2006/06/06. [PubMed: 16751039]
39. Gomes FE, Bentley E, Lin TL, McLellan GJ. Effects of unilateral topical administration of 0.5% tropicamide on anterior segment morphology and intraocular pressure in normal cats and cats with primary congenital glaucoma. Veterinary ophthalmology. 2011; 14(Suppl 1):75–83. Epub 2011/09/23. [PubMed: 21923827]
40. Strouthidis NG, Fortune B, Yang H, Sigal IA, Burgoyne CF. Effect of acute intraocular pressure elevation on the monkey optic nerve head as detected by spectral domain optical coherence tomography. Investigative ophthalmology & visual science. 2011; 52(13):9431–7. Epub 2011/11/08. [PubMed: 22058335]
41. Yamauchi Y, Agawa T, Tsukahara R, Kimura K, Yamakawa N, Miura M, et al. Correlation between high-resolution optical coherence tomography (OCT) images and histopathology in an iodoacetic acid-induced model of retinal degeneration in rabbits. British Journal of Ophthalmology. 2011; 95(8):1157–60. [PubMed: 21030415]
42. Cong L, Sun D, Zhang Z, Jiao W, Rizzolo LJ, Peng S. A Novel Rabbit Model for Studying RPE Transplantation. Investigative ophthalmology & visual science. 2008; 49(9):4115–25. [PubMed: 18502985]
43. Ameri H, Kim JG, Ratanapakorn T, Chader GJ, Humayun MS. Intravitreal and subretinal injection of tissue plasminogen activator (tPA) in the treatment of experimentally created retinal vein occlusion in rabbits. Retina. 2008; 28(2):350–5. Epub 2008/02/28. [PubMed: 18301042]
44. Calderone L, Grimes P, Shalev M. Acute reversible cataract induced by xylazine and by ketamine-xylazine anesthesia in rats and mice. Experimental eye research. 1986; 42(4):331–7. [PubMed: 3754819]
45. Ridder W 3rd, Nusinowitz S, Heckenlively JR. Causes of cataract development in anesthetized mice. Experimental eye research. 2002; 75(3):365–70. [PubMed: 12384099]
46. Bermudez MA, Vicente AF, Romero MC, Arcos MD, Abalo JM, Gonzalez F. Time course of cold cataract development in anesthetized mice. Current eye research. 2011; 36(3):278–84. Epub 2011/02/01. [PubMed: 21275518]
47. Vieira AC, Vicente AF, Perez R, Gonzalez F. Chloral hydrate anesthesia and lens opacification in mice. Current eye research. 2009; 34(5):355–9. Epub 2009/04/30. [PubMed: 19401878]
48. Nagata A, Higashide T, Ohkubo S, Takeda H, Sugiyama K. In Vivo Quantitative Evaluation of the Rat Retinal Nerve Fiber Layer with Optical Coherence Tomography. Investigative ophthalmology & visual science. 2009; 50(6):2809–15. [PubMed: 19182247]
49. Albert DM, Neekhra A, Wang S, Darjatmoko SR, Sorenson CM, Dubielzig RR, et al. Development of choroidal neovascularization in rats with advanced intense cyclic light-induced retinal degeneration. Archives of ophthalmology. 2010; 128(2):212–22. Epub 2010/02/10. [PubMed: 20142545]
50. Seiler MJ, Rao B, Aramant RB, Yu L, Wang Q, Kitayama E, et al. Three-dimensional optical coherence tomography imaging of retinal sheet implants in live rats. Journal of neuroscience methods. 2010; 188(2):250–7. Epub 2010/03/12. [PubMed: 20219535]

51. Gekeler F, Szurman P, Grisanti S, Weiler U, Claus R, Greiner TO, et al. Compound subretinal prostheses with extra-ocular parts designed for human trials: successful long-term implantation in pigs. Graefe's archive for clinical and experimental ophthalmology = Albrecht von Graefes Archiv fur klinische und experimentelle Ophthalmologie. 2007; 245(2):230–41. Epub 2006/04/29. [PubMed: 16645861]
52. Volker M, Shinoda K, Sachs H, Gmeiner H, Schwarz T, Kohler K, et al. In vivo assessment of subretinally implanted microphotodiode arrays in cats by optical coherence tomography and fluorescein angiography. Graefe's archive for clinical and experimental ophthalmology = Albrecht von Graefes Archiv fur klinische und experimentelle Ophthalmologie. 2004; 242(9):792–9. Epub 2004/06/05. [PubMed: 15179515]
53. Güven D, Weiland JD, Maghribi M, Davidson JC, Mahadevappa M, Roizenblatt R, et al. Implantation of an inactive epiretinal poly(dimethyl siloxane) electrode array in dogs. Experimental eye research. 2006; 82(1):81–90. [PubMed: 16125701]
54. Gekeler F, Gmeiner H, Volker M, Sachs H, Messias A, Eule C, et al. Assessment of the posterior segment of the cat eye by optical coherence tomography (OCT). Veterinary ophthalmology. 2007; 10(3):173–8. Epub 2007/04/21. [PubMed: 17445079]
55. Beltran WA, Cideciyan AV, Lewin AS, Iwabe S, Khanna H, Sumaroka A, et al. Gene therapy rescues photoreceptor blindness in dogs and paves the way for treating human X-linked retinitis pigmentosa. Proceedings of the National Academy of Sciences. 2012; 109(6):2132–7.
56. Lheriteau E, Libeau L, Stieger K, Deschamps JY, Mendes-Madeira A, Provost N, et al. The RPGRIP1-deficient dog, a promising canine model for gene therapy. Molecular vision. 2009; 15:349–61. Epub 2009/02/19. [PubMed: 19223988]
57. Cideciyan AV, Jacobson SG, Aleman TS, Gu D, Pearce-Kelling SE, Sumaroka A, et al. In vivo dynamics of retinal injury and repair in the rhodopsin mutant dog model of human retinitis pigmentosa. Proceedings of the National Academy of Sciences of the United States of America. 2005; 102(14):5233–8. [PubMed: 15784735]
58. Schallek JB, McLellan GJ, Viswanathan S, Ts'o DY. Retinal Intrinsic Optical Signals in a Cat Model of Primary Congenital Glaucoma. Investigative ophthalmology & visual science. 2012 Epub 2012/03/08.
59. Grozdanic SD, Matic M, Betts DM, Sakaguchi DS, Kardon RH. Recovery of canine retina and optic nerve function after acute elevation of intraocular pressure: implications for canine glaucoma treatment. Veterinary ophthalmology. 2007; 10(Suppl 1):101–7. Epub 2007/11/29. [PubMed: 17973841]
60. Savini G, Barboni P, Carbonelli M, Sbreglia A, Deluigi G, Parisi V. Comparison of Optic Nerve Head Parameter Measurements Obtained by Time-domain and Spectral-domain Optical Coherence Tomography. Journal of glaucoma. 2012 Epub 2012/03/01.
61. Sung KR, Kim DY, Park SB, Kook MS. Comparison of retinal nerve fiber layer thickness measured by Cirrus HD and Stratus optical coherence tomography. Ophthalmology. 2009; 116(7): 1264–70. 70, e1. Epub 2009/05/12. [PubMed: 19427696]
62. Knight OJ, Chang RT, Feuer WJ, Budenz DL. Comparison of retinal nerve fiber layer measurements using time domain and spectral domain optical coherent tomography. Ophthalmology. 2009; 116(7):1271–7. Epub 2009/04/28. [PubMed: 19395086]
63. Leung CK, Cheung CY, Weinreb RN, Qiu Q, Liu S, Li H, et al. Retinal nerve fiber layer imaging with spectral-domain optical coherence tomography: a variability and diagnostic performance study. Ophthalmology. 2009; 116(7):1257–63. 63, e1–2. Epub 2009/05/26. [PubMed: 19464061]
64. Sull AC, Vuong LN, Price LL, Srinivasan VJ, Gorczynska I, Fujimoto JG, et al. Comparison of spectral/Fourier domain optical coherence tomography instruments for assessment of normal macular thickness. Retina. 2010; 30(2):235–45. Epub 2009/12/03. [PubMed: 19952997]
65. Chong GT, Farsiu S, Freedman SF, Sarin N, Koreishi AF, Izatt JA, et al. Abnormal foveal morphology in ocular albinism imaged with spectral-domain optical coherence tomography. Archives of ophthalmology. 2009; 127(1):37–44. Epub 2009/01/14. [PubMed: 19139336]
66. Hong S, Kim CY, Seong GJ. Adjusted peripapillary retinal nerve fiber layer thickness measurements based on the optic nerve head scan angle. Investigative ophthalmology & visual science. 2010; 51(8):4067–74. Epub 2010/03/20. [PubMed: 20237251]

67. Han IC, Jaffe GJ. Evaluation of artifacts associated with macular spectral-domain optical coherence tomography. Ophthalmology. 2010; 117(6):1177–89. e4. Epub 2010/02/23. [PubMed: 20171740]
68. Gabriele ML, Ishikawa H, Wollstein G, Bilonick RA, Townsend KA, Kagemann L, et al. Optical coherence tomography scan circle location and mean retinal nerve fiber layer measurement variability. Investigative ophthalmology & visual science. 2008; 49(6):2315–21. Epub 2008/06/03. [PubMed: 18515577]
69. Vizzeri G, Bowd C, Medeiros FA, Weinreb RN, Zangwill LM. Effect of signal strength and improper alignment on the variability of stratus optical coherence tomography retinal nerve fiber layer thickness measurements. American journal of ophthalmology. 2009; 148(2):249–55. e1. Epub 2009/05/12. [PubMed: 19427621]
70. Ho J, Castro DP, Castro LC, Chen Y, Liu J, Mattox C, et al. Clinical assessment of mirror artifacts in spectral-domain optical coherence tomography. Investigative ophthalmology & visual science. 2010; 51(7):3714–20. Epub 2010/02/26. [PubMed: 20181840]
71. Kang SH, Hong SW, Im SK, Lee SH, Ahn MD. Effect of myopia on the thickness of the retinal nerve fiber layer measured by Cirrus HD optical coherence tomography. Investigative ophthalmology & visual science. 2010; 51(8):4075–83. Epub 2010/03/20. [PubMed: 20237247]
72. Rauscher FM, Sekhon N, Feuer WJ, Budenz DL. Myopia affects retinal nerve fiber layer measurements as determined by optical coherence tomography. Journal of glaucoma. 2009; 18(7): 501–5. Epub 2009/09/12. [PubMed: 19745664]
73. Asrani S, Edghill B, Gupta Y, Meerhoff G. Optical coherence tomography errors in glaucoma. Journal of glaucoma. 2010; 19(4):237–42. Epub 2009/08/08. [PubMed: 19661819]
74. Yang Q, Reisman CA, Wang Z, Fukuma Y, Hangai M, Yoshimura N, et al. Automated layer segmentation of macular OCT images using dual-scale gradient information. Optics express. 2010; 18(20):21293–307. Epub 2010/10/14. [PubMed: 20941025]
75. Hu Z, Niemeijer M, Abramoft MD, Lee K, Garvin MK. Automated segmentation of 3-D spectral OCT retinal blood vessels by neural canal opening false positive suppression. Medical image computing and computer-assisted intervention: MICCAI International Conference on Medical Image Computing and Computer-Assisted Intervention. 2010; 13(Pt 3):33–40. Epub 2010/10/01. [PubMed: 20879380]
76. Debuc DC, Salinas HM, Ranganathan S, Tatrai E, Gao W, Shen M, et al. Improving image segmentation performance and quantitative analysis via a computer-aided grading methodology for optical coherence tomography retinal image analysis. Journal of biomedical optics. 2010; 15(4):046015. Epub 2010/08/31. [PubMed: 20799817]
77. Roberts MD, Liang Y, Sigal IA, Grimm J, Reynaud J, Bellezza A, et al. Correlation between local stress and strain and lamina cribrosa connective tissue volume fraction in normal monkey eyes. Investigative ophthalmology & visual science. 2010; 51(1):295–307. Epub 2009/08/22. [PubMed: 19696175]
78. Sigal IA, Ethier CR. Biomechanics of the optic nerve head. Experimental eye research. 2009; 88(4):799–807. Epub 2009/02/17. [PubMed: 19217902]
79. DeBuc, DC. A Review of Algorithms for Segmentation of Retinal Image Data Using Optical Coherence Tomography. In: Ho, P-G., editor. Image Segmentation. InTech; 2011. p. 15-54.
80. Wu Z, Vazeen M, Varma R, Chopra V, Walsh AC, LaBree LD, et al. Factors Associated with Variability in Retinal Nerve Fiber Layer Thickness Measurements Obtained by Optical Coherence Tomography. Ophthalmology. 2007; 114(8):1505–12. [PubMed: 17367862]
81. Sung KR, Wollstein G, Schuman JS, Bilonick RA, Ishikawa H, Townsend KA, et al. Scan quality effect on glaucoma discrimination by glaucoma imaging devices. The British journal of ophthalmology. 2009; 93(12):1580–4. Epub 2009/08/21. [PubMed: 19692363]
82. Mwanza JC, Durbin MK, Budenz DL, Sayyad FE, Chang RT, Neelakantan A, et al. Glaucoma Diagnostic Accuracy of Ganglion Cell-Inner Plexiform Layer Thickness: Comparison with Nerve Fiber Layer and Optic Nerve Head. Ophthalmology. 2012 Epub 2012/03/01.
83. Iwama D, Hangai M, Ooto S, Sakamoto A, Nakanishi H, Fujimura T, et al. Automated Assessment of Drusen Using Three-dimensional Spectral-domain Optical Coherence Tomography. Investigative ophthalmology & visual science. 2012 Epub 2012/02/03.

84. Hahn P, Migacz J, O'Connell R, Maldonado RS, Izatt JA, Toth CA. The use of optical coherence tomography in intraoperative ophthalmic imaging. Ophthalmic surgery, lasers & imaging: the official journal of the International Society for Imaging in the Eye. 2011; 42(Suppl):S85–94. Epub 2011/07/28.

85. Tao YK, Ehlers JP, Toth CA, Izatt JA. Intraoperative spectral domain optical coherence tomography for vitreoretinal surgery. Optics letters. 2010; 35(20):3315–7. Epub 2010/10/23. [PubMed: 20967051]

86. Ehlers JP, Tao YK, Farsiu S, Maldonado R, Izatt JA, Toth CA. Integration of a spectral domain optical coherence tomography system into a surgical microscope for intraoperative imaging. Investigative ophthalmology & visual science. 2011; 52(6):3153–9. Epub 2011/02/02. [PubMed: 21282565]

87. Kocaoglu OP, Cense B, Jonnal RS, Wang Q, Lee S, Gao W, et al. Imaging retinal nerve fiber bundles using optical coherence tomography with adaptive optics. Vision research. 2011; 51(16): 1835–44. Epub 2011/07/05. [PubMed: 21722662]

88. Godara P, Siebe C, Rha J, Michaelides M, Carroll J. Assessing the photoreceptor mosaic over drusen using adaptive optics and SD-OCT. Ophthalmic surgery, lasers & imaging: the official journal of the International Society for Imaging in the Eye. 2010; 41(Suppl):S104–8. Epub 2010/12/02.

89. Zawadzki RJ, Jones SM, Pilli S, Balderas-Mata S, Kim DY, Olivier SS, et al. Integrated adaptive optics optical coherence tomography and adaptive optics scanning laser ophthalmoscope system for simultaneous cellular resolution in vivo retinal imaging. Biomedical optics express. 2011; 2(6): 1674–86. Epub 2011/06/24. [PubMed: 21698028]

90. Srinivasan VJ, Adler DC, Chen Y, Gorczynska I, Huber R, Duker JS, et al. Ultrahigh-speed optical coherence tomography for three-dimensional and en face imaging of the retina and optic nerve head. Investigative ophthalmology & visual science. 2008; 49(11):5103–10. Epub 2008/07/29. [PubMed: 18658089]

91. Yang H, Qi J, Hardin C, Gardiner SK, Strouthidis NG, Fortune B, et al. Spectral domain optical coherence tomography (SDOCT) enhanced depth imaging (EDI) of the normal and glaucomatous non-human primate (NHP) optic nerve head (ONH). Investigative ophthalmology & visual science. 2011 Epub December 9, 2011.

92. Baumann B, Potsaid B, Kraus MF, Liu JJ, Huang D, Hornegger J, et al. Total retinal blood flow measurement with ultrahigh speed swept source/Fourier domain OCT. Biomedical optics express. 2011; 2(6):1539–52. Epub 2011/06/24. [PubMed: 21698017]

93. Wang Y, Fawzi AA, Varma R, Sadun AA, Zhang X, Tan O, et al. Pilot study of optical coherence tomography measurement of retinal blood flow in retinal and optic nerve diseases. Investigative ophthalmology & visual science. 2011; 52(2):840–5. Epub 2010/11/06. [PubMed: 21051715]

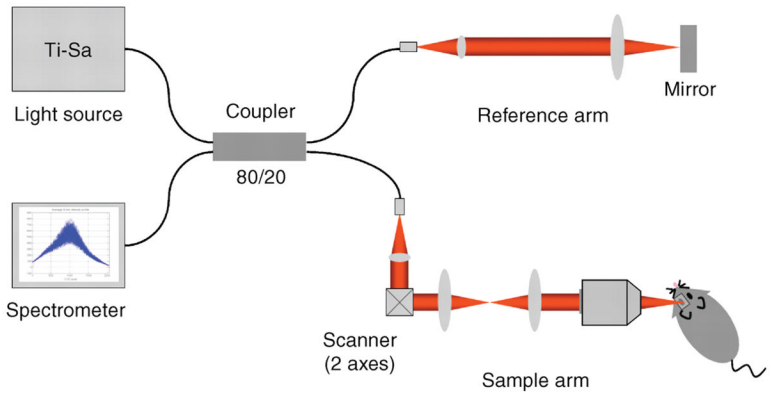

Figure 1.

Schematic of a high-resolution SD-OCT system for mouse retinal imaging. The system is based on a fiber coupler. Broadband light from the Ti-Sa laser is split into both the reference arm and sample arm. Back-scattered light from the retina is coupled back to the fiber, combined with reflected light from the reference arm at the coupler, and delivered to the spectrometer. Light in the air is depicted in red. (Reproduced with permission from: Kim KH, Puoris'haag M, Maguluri GN, et al. Monitoring mouse retinal degeneration with high-resolution spectral-domain optical coherence tomography. *Journal of Vision*, 2008 Jan 24;8(1):17.1–11)

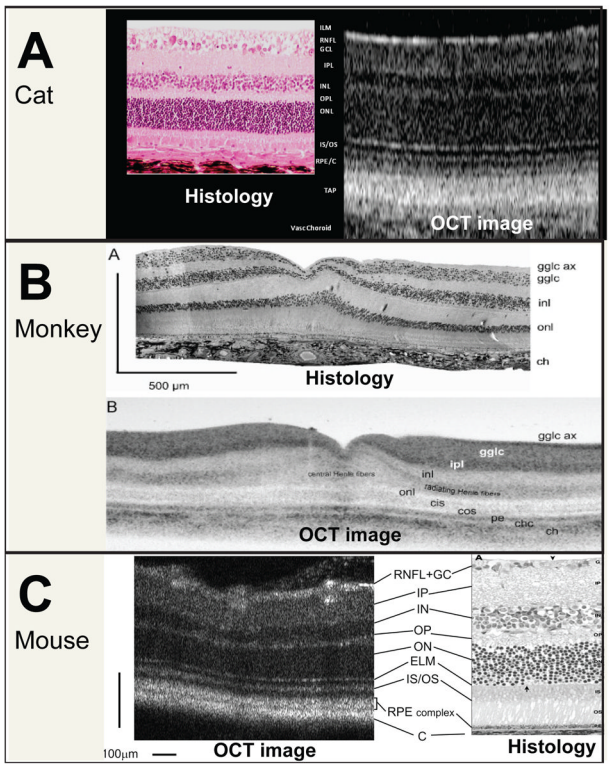

Figure 2.

Comparison of OCT cross-sectional images with retinal layers identifiable on histology. Normal adult **CAT:** photomicrograph on left and spectral domain OCT scan on right. Internal limiting membrane/retinal nerve fiber layer (ILM/RNFL); ganglion cell layer (GCL); inner plexifom layer (IPL); dark band of inner nuclear layer (INL); outer plexiform layer (OPL); dark band of outer nuclear layer (ONL); junction of the inner segments and outer segments (IS/OS) RPE and choriocapillaris (RPE/C); tapetum (TAP); vascular choroid (Vasc Choroid). Normal **MONKEY:** Ganglion cell axons (gglc ax); ganglion cell body layer (gglc); inner plexiform layer (ipl); inner nuclear layer (inl); outer plexiform layer (transition between Henle fibers and inl; not labeled); outer nuclear layer (onl); foveal cone inner segments (cis); foveal cone outer segments (cos); pigment epithelium+processes (pe); choriocapillaris (chc); choroid (ch) (Reproduced with permission from Drexler W, Fujimoto JG. State-of-the-art retinal optical coherence tomography Prog Retin Eye Res. 2008 Jan; 27(1):45–88.) Normal **MOUSE**: retinal nerve fiber layer (RNFL); ganglion cell layer (GC); inner plexiform layer (IP); inner nuclear layer (IN); outer plexiform layer (OP); outer nuclear layer (ON); external limiting membrane (ELM); junction between the inner and outer segment of the photoreceptors (IS/OS); retinal pigment epithelium (RPE) complex; choroid (C). (Reproduced, with permission, from Ruggeri M, Wehbe H, Jiao S, et al. In vivo three-dimensional high-resolution imaging of rodent retina with spectral-domain optical coherence tomography. Invest Ophthalmol Vis Sci. 2007 Apr;48(4):1808–14.

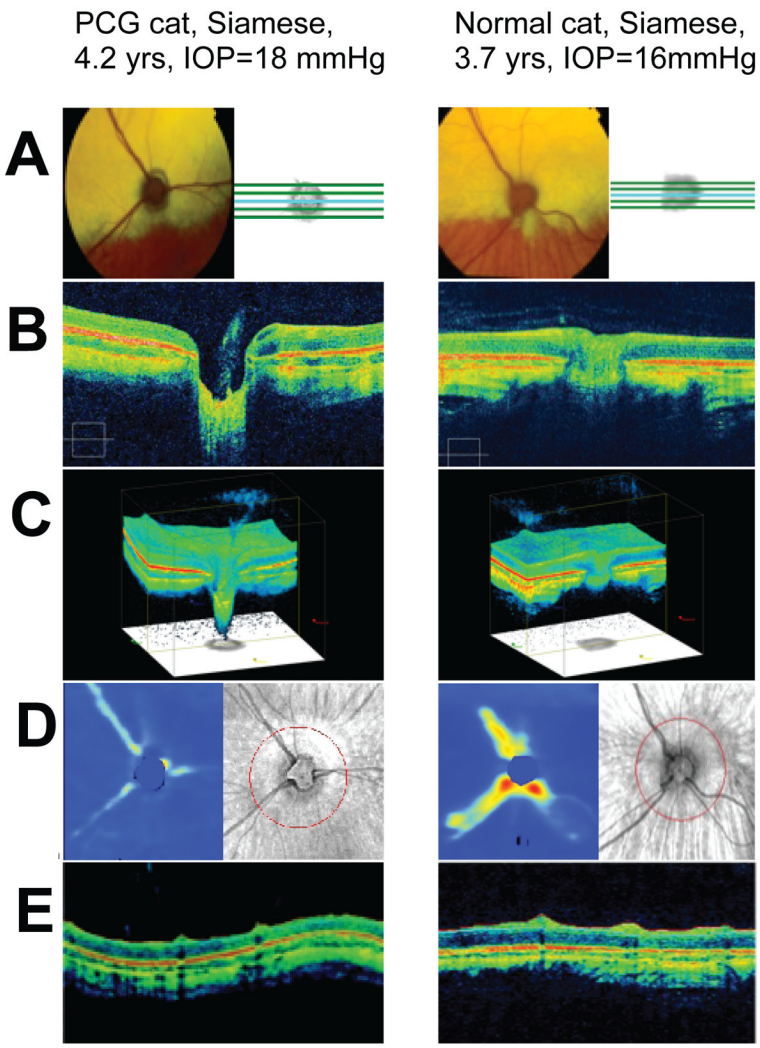

Figure 3.

Representative SD-OCT images of the left eyes of normal and glaucomatous adult Siamese cats illustrate cupping of the optic nerve head and thinning of the retinal nerve fiber layer (RNFL) resulting from feline congenital glaucoma. Fundus photographs and corresponding reflectance images **(A)** illustrate the scan line location of raster scans **(B).** 3D optic disc cubes are shown in **(C),** with retinal nerve fiber layer thickness maps below, in which thicker areas are depicted in warmer colors and thinner areas in cooler colors **(D).** Adjacent reflectance images illustrate location of scan circles. In the Optic disc cube/RNFL tomograms **(E),** temporal-superior-nasal-inferior- temporal quadrants (“TSNIT”) are represented from left to right of images.

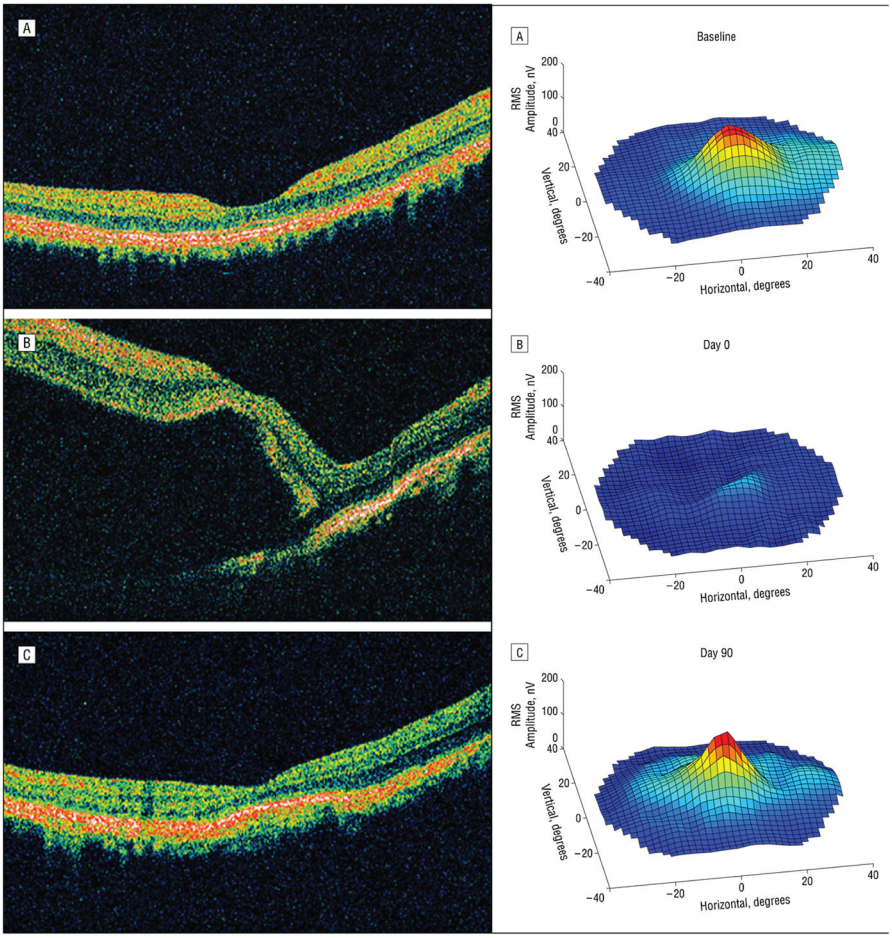

Figure 4.

In a monkey sub-retinal injection model, structural abnormalities identified by OCT (left) were associated with functional deficits in the multifocal electroretinogram (mfERG; right). Compared to baseline **(A),** focal retinal detachment and marked reduction in mfERG responses could be seen immediately post- injection **(B)** but were largely resolved by 2 days post-injection. Retinal function was nearly recovered by three months post injection **(C),** although organization of the outer segments remained disrupted, highlighting the need to separate procedural effects from drug effects when using novel techniques. Reproduced, with permission, from Nork TM, Murphy CJ, Kim CB, et al. Functional and anatomic consequences of subretinal dosing in the cynomolgus macaque. Archives of ophthalmology. 2012;130(1):65–75.

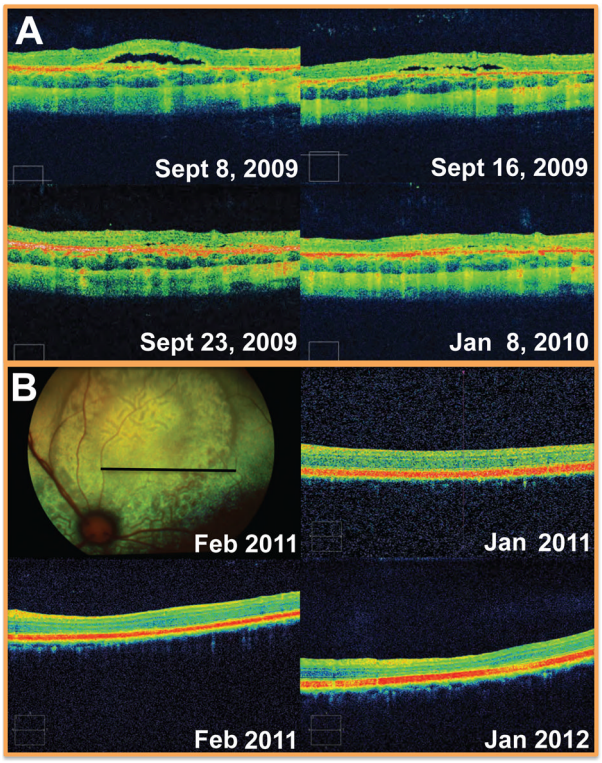

Figure 5.

Monitoring structural abnormalities over time. **A** focal, flat retinal separation was identified as an incidental finding when scanning a Siamese cat as part of a longitudinal study. The lesion, which was located in the non-tapetal fundus, was not visualized on ophthalmoscopy but was followed by SD-OCT scanning as it spontaneously resolved over 3 weeks. The underlying cause was not determined. **B:** Sequential OCT scans documented chorioretinal folds in a domestic short haired cat and confirmed that this lesion (which resembles geographic retinal dysplasia in fundus photographs) represents acquired pathology rather than congenital malformation (i.e. retinal dysplasia) as it was not present in earlier scans.

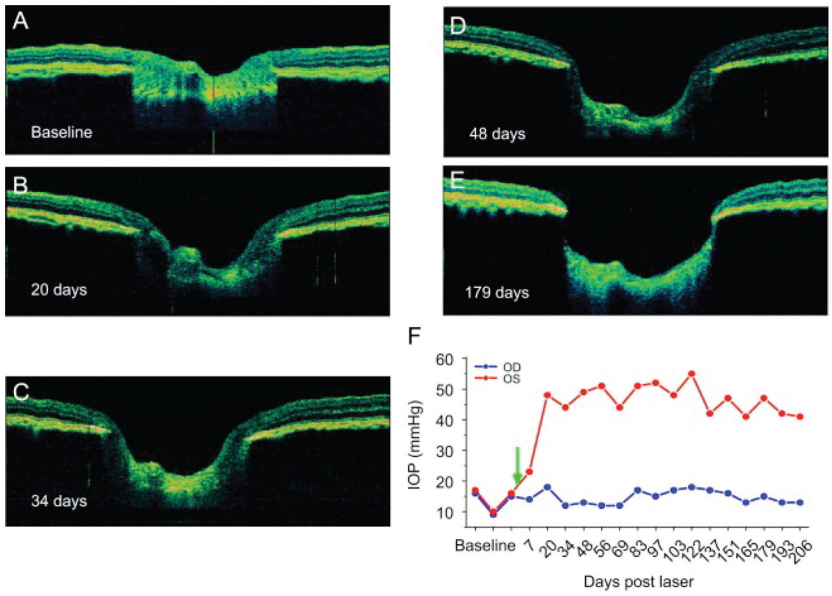

Figure 6.

Monitoring disease progression using in vivo ultra high resolution retinal OCT of the optic nerve head in a non-human primate glaucoma model. Horizontal OCT images of the same eye are depicted at baseline (A), 20 days (B), 34 days (C) 48 days (D) as well as 179 days (E) after induction of unilateral ocular hypertension. Measured intraocular pressure of test (red) and control eye (blue, F). (Reproduced, with permission, from: Drexler W, Fujimoto JG. State-of-the-art retinal optical coherence tomography Prog Retin Eye Res. 2008 Jan; 27(1):45–88.)

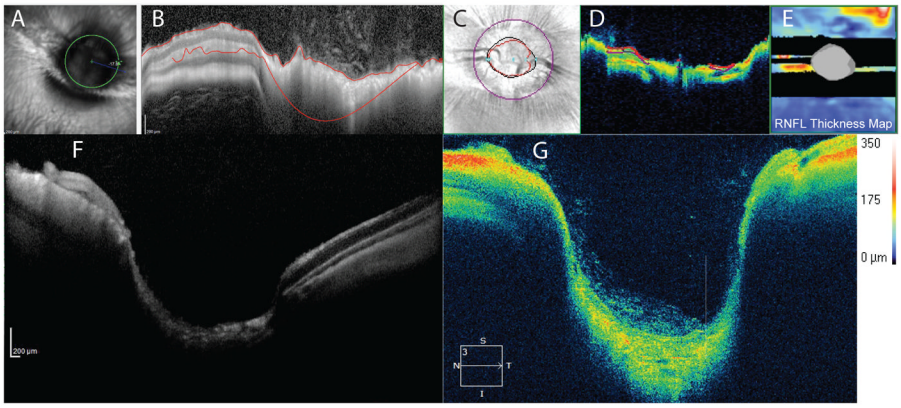

Figure 7.
SD-OCT scans of normal rabbit optic nerve head (ONH) illustrating the unique retinal and ONH anatomy of this species. Scans suitable for qualitative analysis can be obtained (F and G) but software designed for human subjects may not be scaled appropriately to fully encompass the large, deeply cupped optic nerve head (A and C) or segment RNFL thickness accurately (B and D). Note the black bands, with lack of signal corresponding to the medullary rays, in the RNFL thickness map (E).

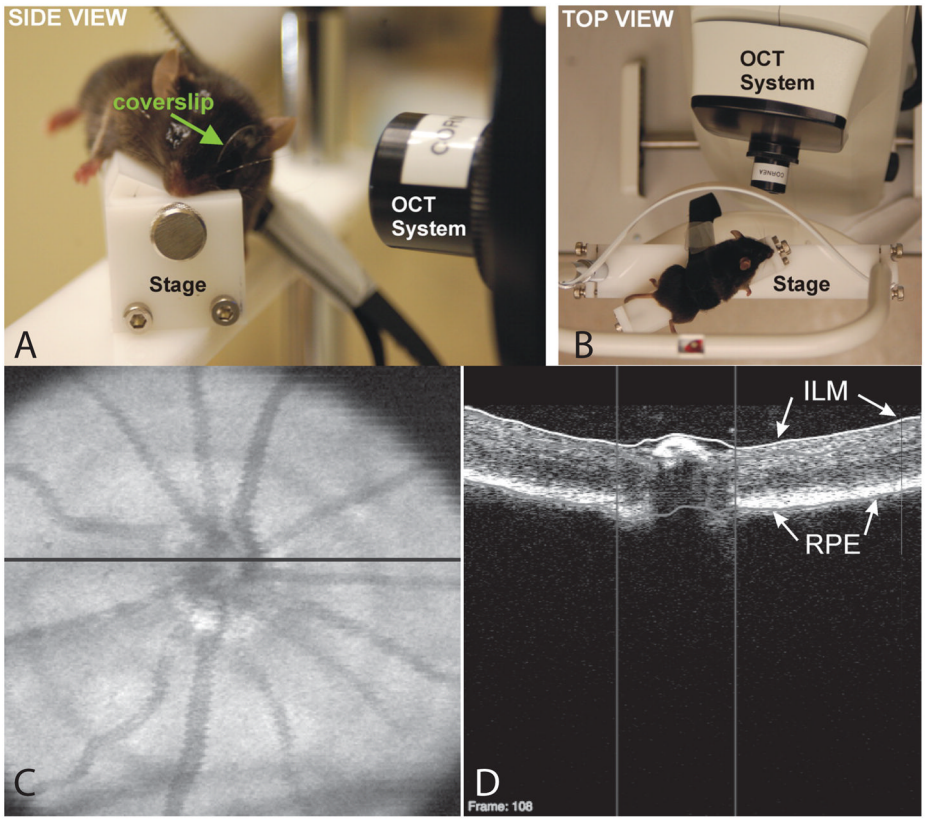

Figure 8.

A: Side (left) and B: top (right) views of the stage used to align a mouse for SD-OCT imaging of the ONH. A coverslip was used to account for the steep curvature of the mouse cornea and prevent corneal desiccation. C: SD-OCT en face image (left) with the black line indicating the location of the D: OCT B-scan (right). The B-scan demonstrates automated segmentation of the ILM (white line) and RPE (gray line) to obtain measurements. Vertical lines: disc margin. Reproduced, with permission, from Gabriele ML, Ishikawa H, Schuman JS, Bilonick RA, Kim J, Kagemann L, Wollstein G. Reproducibility of spectral-domain optical coherence tomography total retinal thickness measurements in mice. Invest Ophthalmol Vis Sci. 2010 Dec;51(12):6519–23.

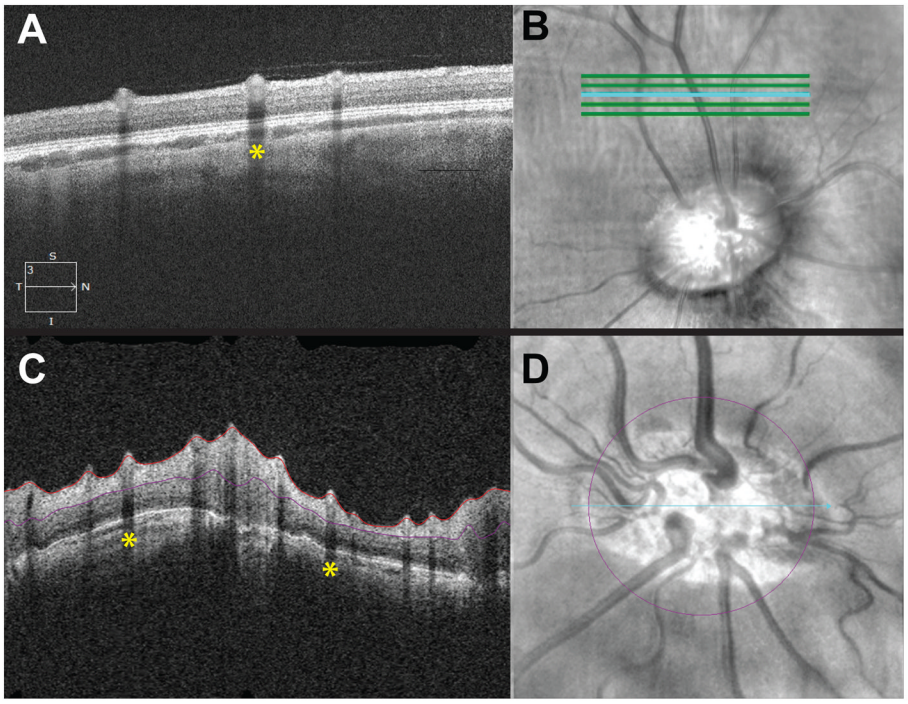

Figure 9.

(A) SD-OCT raster scan of a mini pig retina and (C) SD-OCT RNFL circle scan centered on the optic nerve with corresponding reflectance images (B and D) showing location of scan lines. In both scan types, there is sufficient definition of retinal layers to allow qualitative assessment. The large, oval optic nerve head of the mini pig makes the RNFL circle designed for humans a poor fit, which will impact quantitative RNFL values derived from the optic nerve cube scan. Note that retinal blood vessels, relatively prominent in this species, are associated with characteristic linear “shadows” (yellow stars).

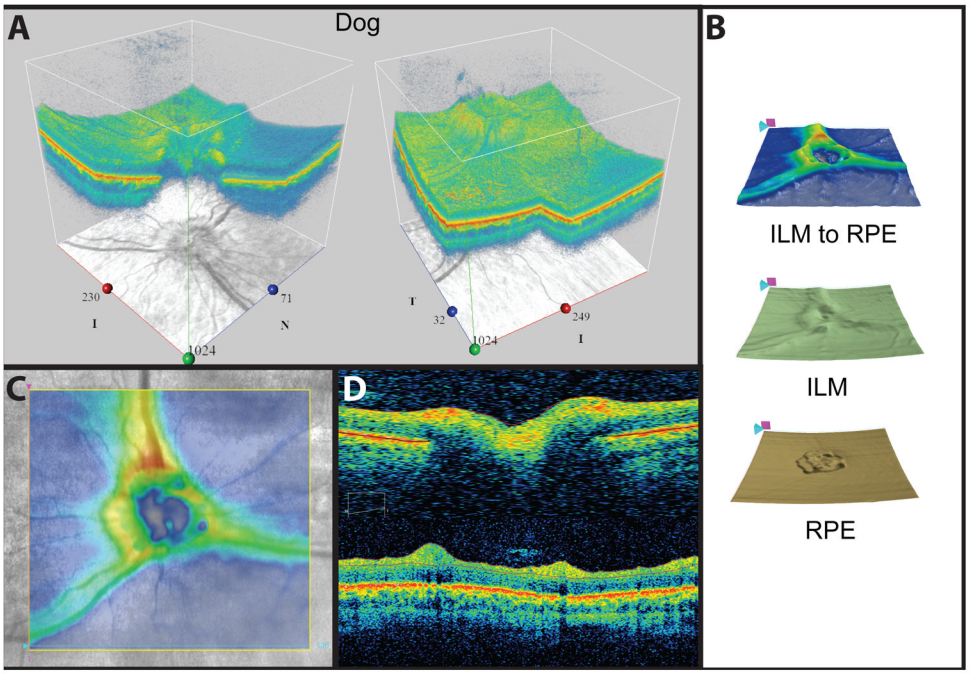

Figure 10.

SD-OCT images obtained from a normal Springer spaniel. Most SD-OCT systems offer a variety of diagnostic analysis tools such as adjustable 3-D views (A), retinal layer mapping (B) and color-coded thickness mapping (C) that can assist with longitudinal qualitative assessments. Line scans (D) through the optic nerve (top) and around the optic nerve head (bottom) show conventional cross sectional views.

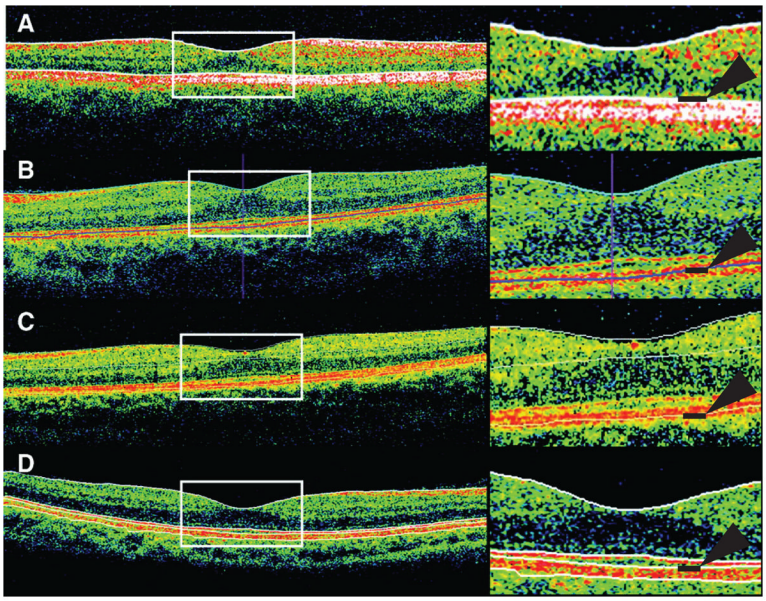

Figure 11.

Demonstration of macular thickness segmentation algorithms in different instruments. All instruments define the inner boundary as the internal limiting membrane, but there is variation in outer boundaries (black lines and arrows). Stratus OCT measures to the IS/OS junction (A), Cirrus HD-OCT (B) and RTVue-100 (C) both measure close to the RPE, and the RTVue also draws a boundary at the inner plexiform layer. 3D OCT-1000 measures to the photoreceptor outer segment tips (D), shown as the third line from the top. This instrument also draws boundaries at the IS/OS junction (second line) and posterior RPE boundary (fourth line), which are not included in retinal thickness measurements. (Adapted with permission, from: Sull AC, Vuong LN, Price LL, et al. Comparison of spectral/Fourier domain optical coherence tomography instruments for assessment of normal macular thickness. Retina. 2010 Feb; 30 (2):235–45.)

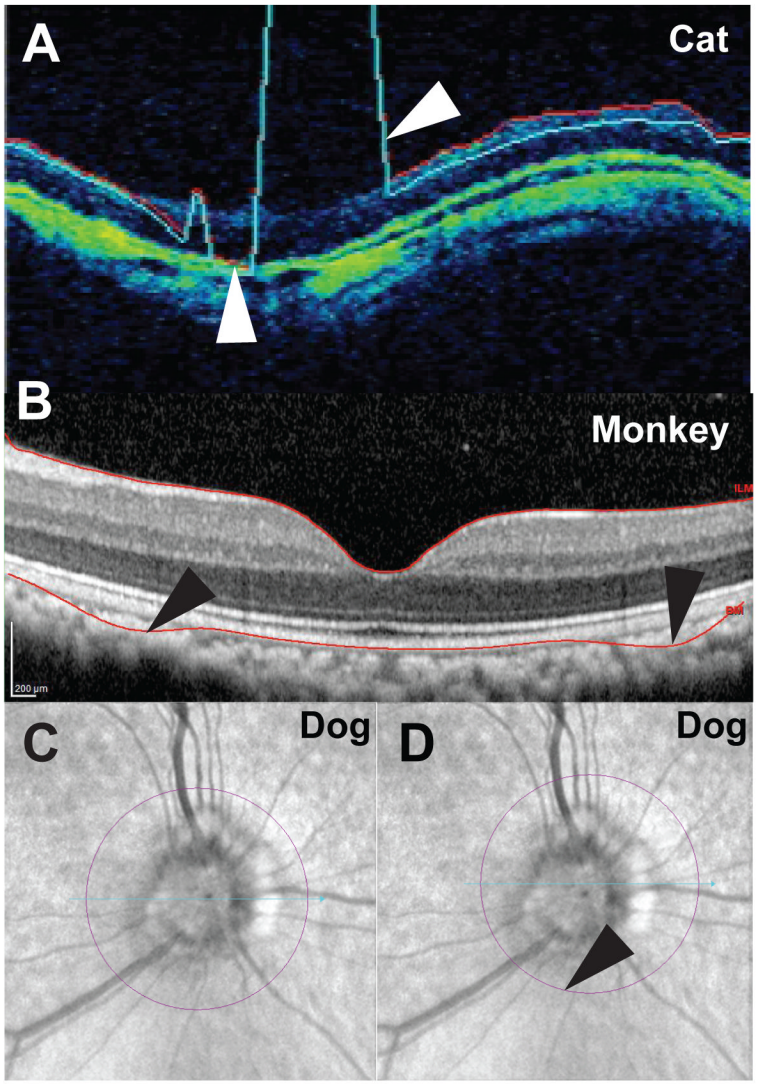

Figure 12.
Commonly encountered segmentation errors include A: Failure to properly delineate the inner retinal surface of the RNFL (white arrows) in a cat with glaucoma, in association with poor and uneven signal strength. B: Failure to accurately delineate the outer retinal surfaces in a macaque macula (black arrows), despite high signal strength. C: Normal adult dog reflectance image showing a centered optic nerve circle and D: Off-center optic nerve circle (black arrow) that had to be corrected manually.

Table 1

List and description of commercially available SD- OCT systems.

Device	Manufacturer	Axial resolution (μm)	A-scan acquisition Rate	Description of Capabilities
Spectralis HRA + OCT[a]	Heidelberg Engineering, Heidelberg, Germany	3.5(digital)	40 000/sec	Various models offer eye tracking, FA, ICG, cSLO, AF, IR; rodentand AS options; wide angle
Cirrus HD-OCT	Carl Zeiss Meditec, Dublin, CA, USA	5	27 000/sec	ILM, RPE retinal layer maps, guided progression analysis for glaucoma; eye tracking; AS option
SD-OIS	Bioptigen, Research Triangle Park, NC, USA	4	17 000/sec	Designed for clinical and animal research use; includes hand-held scannerand microscope set up; rodent option; various animal holders, stages etc; IR; AS option
EnvisuSD-OIS series	Bioptigen, Research Triangle Park, NC, USA	2–3	34 000/sec	R-class iscurrently pre-clinical/research use only; C class is approved for clinical use in Europe and Canada; Doppler flow; EDI; rodent options
RTVue-100	Optovue, Fremont, CA, USA	5	26 000/sec	Multiple glaucoma scanning protocols; eye tracking; IR fundus; cornea power measurements
iVue	Optovue, Fremont, CA, USA	5	26 000/sec	Compact; optional stand allows scan angle to be altered.
3D-OCT 2000	Topcon, Tokyo, Japan	6	27000/sec	Color fundus photography; FA; AF, AS attachment available
SL Scan-1	Topcon, Tokyo, Japan	8–9	5000/sec	Table mounted slit lamp; AS; optional digital camera and lens holder for fundus imaging.
SOCT Copernicus	Optopol, Zawierce, Poland	6	25 000/sec	Glaucoma progression analysis software; IR
SOCT HR Copernicus[b]	Optopol, Zawierce, Poland	3	52 000/sec	Glaucoma module; IR; AS module; retina tracking system
Spectral OCT SLO	Optos plc, Dunfermline, UK[c]	<6	27 000/sec	Combines microperimetry & cSLO; eye tracking; AS option

(FA = fluorescein angiography; ICG = indocyanine green angiography; cLSO = confocal laser scanning ophthalmoscopy; AF= autofluorescence imaging; IR = infrared imaging; AS= anterior segment OCT imaging).

[a] various models/options available and are hardware upgradeable with exception of basic “Spectralis OCT” model, which also has a fixed, rather than panning, camera head;

[b] Copernicus-HR system (in development) expected to offer 3μm axial resolution; Doppler blood flow analysis, and acquisition rate of 50000 A-scans/sec;

[c] formerly manufactured by Opko, Miami, FL, USA. Adapted from *Gabriele et al, Invest Ophthalmol Vis Sci.* 2011;52:2425–243 and *Keirnan, D.F, Meiler, W.F. and Hariprasad, S. M., Am J Opthalmol 2010; 149:18–31* with additional information from manufacturers’ websites.